

Ionized Gas in the Sgr A Complex - VLA Observations of H168 α and H270 α Recombination Lines

K.R. Anantharamaiah^{1,2}, A. Pedlar³ and W.M. Goss¹

¹*National Radio Astronomy Observatory, Socorro, NM 87801, USA*

²*Raman Research Institute, Bangalore 560 080, India*

³*Nuffield Radio Astronomy Laboratories, Jodrell Bank, UK*

Abstract. Radio recombination lines at $\lambda = 20$ cm reveals the presence of an extended component of ionized gas of lower density (~ 100 cm⁻³) in the Sgr A complex. This component extends well beyond the thermal ‘mini-spiral’ SgrA-West which seem to be embedded in it. The low-density component is present over the entire extent of SgrA East and possibly beyond and it is responsible for the turnover in the spectrum of SgrA East and the halo observed by Pedlar et al (1989) at $\lambda = 90$ cm. The radial velocity of the extended ionized gas range from $+50$ km s⁻¹ to -200 km s⁻¹ with minima of emission near -50 and -150 km s⁻¹. The total mass of the low-density component is estimated to be $\sim 10^4$ M $_{\odot}$. A possible extended feature at a high velocity of 470 km s⁻¹ is also detected, but needs further observations to confirm it.

1. Introduction

At centimeter wavelengths, most of the radio continuum emission from the Sgr A complex arises from four distinct components: (1) the ultra-compact non-thermal radio source SgrA* which may be at the very center of the Galaxy (Lo et al 1998), (2) the ‘mini-spiral’ SgrA West which is a rotating ionized ring around SgrA* (Ekers et al 1983, Roberts and Goss 1993) (3) the shell-type, non-thermal source SgrA East which is possibly an energetic supernova remnant, located off-centered on SgrA* (Ekers et al 1983) and (4) a triangular shaped halo which seem to surround all the other three components (Pedlar et al 1989). In addition to these four main components, the SgrA complex also contains many weaker but distinct thermal and non-thermal radio features which have been classified and cataloged by Yusef-Zadeh and Morris (1987)

Using high resolution observations at 90 cm and 20 cm, Pedlar et al (1989) obtained constraints on the relative location along the line of sight of the main components of the Sgr A complex. They showed clearly that much of the thermal gas associated with SgrA West lies in front of SgrA* and SgrA East. Fig 1a shows a 20 cm image of the SgrA region. The large shell like structure is SgrA East. The bright compact source within the shell and the bright extended region around it consists of SgrA* and SgrA West. At this resolution ($10'' \times 8''$), SgrA* is not separated from SgrA West and the mini-spiral-like structure of SgrA West

is not resolved. Fig 1b shows an image of the same region at 90 cm with the same angular resolution. The difference between the structures in Figs 1a and 1b is remarkable. The change in the structure is caused by the different emission mechanisms for SgrA West and SgrA East (thermal and non-thermal) and their relative location along the line of sight. The thermal source SgrA West is seen as a depression in Fig 1b whereas it appears as a bright emission feature superposed over the non-thermal source SgrA East in Fig 1a. The conclusion is obvious - SgrA West is in front of SgrA East and the former has become optically thick at $\lambda = 90$ cm and thus absorbs the radiation from the non-thermal source SgrA East.

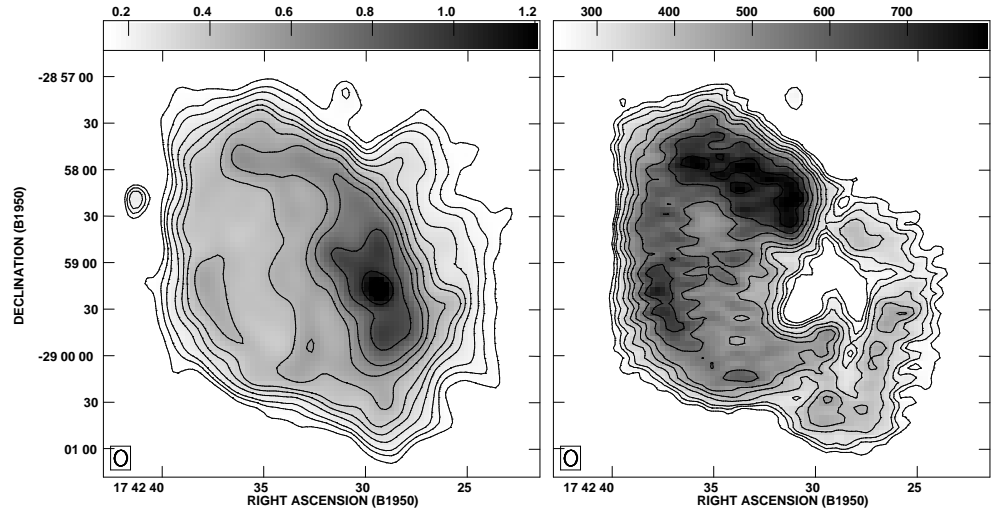


Figure 1. (a) A 20 cm image of the SgrA region. Contour levels are 150, 175, 200, 250, 300, 350, 450 ... 1250 mJy/beam. (b) A 90 cm image of the same region. Contour levels are 250, 275, 300, 350, 400, 450, 550, 650, 750 mJy/beam. The images are taken from Anantharamaiah et al (1991) and convolved to a resolution of $10'' \times 8''$.

The difference between the emissions at 20 cm and 90 cm is seen quantitatively in Fig 2a, which displays EW cross-cuts through the images in Figs 1a and 1b at the position of SgrA*. At 20 cm (thick line) the minor peak on the east is due to the shell of SgrA East and the strong peak is due to the combination of SgrA* and SgrA West. The strong peak at 20 cm turns to an apparent absorption-like feature at 90 cm (thin line) indicating that both SgrA* and SgrA East are absorbed by the optically thick SgrA West. An important implication of this result is that, *it is not possible to obtain any measurement of the flux density of SgrA* at frequencies below about 500 MHz* and thus no constraints can be placed at these frequencies on theoretical models which try to explain the overall spectrum of SgrA* (e.g. Mahadevan 1998). At these frequencies, SgrA* is simply hidden behind an absorbing screen.

Fig 2b shows an image of the spectral index α (where $S_\nu \propto \nu^\alpha$) of the SgrA region between 20 cm and 90 cm made from the images shown in Fig 1. As expected for optically thick thermal gas, positive spectral indices are

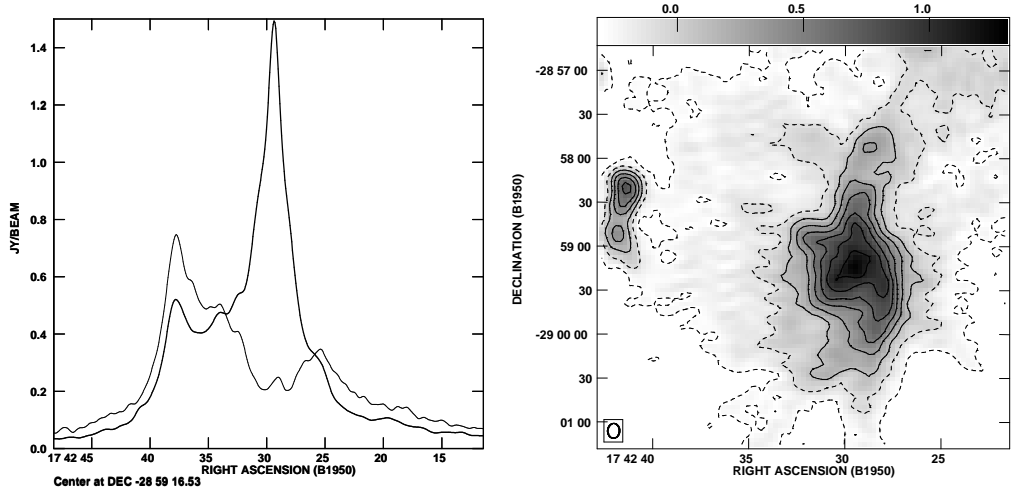


Figure 2. (a) EW cross-cuts at 20 cm (thick line) and 90 cm (thin line) made from Fig 1 at the position of SgrA* (b) An image of the spectral index α (where $S_\nu \propto \nu^\alpha$) of the SgrA region between 90 cm and 20 cm made from the images in Fig 1. The contour levels are -0.3,-0.1,.1,0.3 ... 1.3.

observed over the SgrA West region. In fact the optically thick region seem to extend well beyond the extent of SgrA West as determined by higher frequency observations (Ekers et al 1983). As noted by Pedlar et al (1989), the mini-spiral SgrA West seems to be embedded in a somewhat lower density extended ionized gas. Furthermore, the spectral index of SgrA East and the halo between 20 cm and 90 cm is ‘flatter’ ($\alpha \sim -0.3$ to 0.0) compared to the spectral index between 20 cm and 6 cm ($\alpha \sim -1.1$ to -0.9 : Ekers et al 1983, Pedlar et al 1989) indicating that free-free absorption by thermal gas causes the turnover in their non-thermal spectrum. A quantitative estimate of the amount of thermal gas in front of SgrA East and also in the halo was made by Pedlar et al (1989) using high resolution images at 2 cm, 6 cm, 20 cm and 90 cm. They showed that (1) the mini-spiral of SgrA West is embedded in a thermal-halo, about 1.5 arcmin in angular extent and a ionized gas mass of $\sim 500M_\odot$ and (2) ionized gas with an emission measures $\sim 10^5 \text{ pc cm}^{-6}$ and $\tau_{90\text{cm}} \sim 1$ is present over the extent of SgrA East ($\sim 3'$) and possibly beyond and (3) the triangular-shaped halo surrounding both SgrA East and SgrA West is possibly a mixture of thermal and non-thermal gas and may be responsible for part or all of the spectral turnover of SgrA East between 20 cm and 90 cm.

In this paper, we report observations of recombination lines at 20 cm and 90 cm using the VLA. The 20 cm data clearly shows the presence of non-zero velocity ionized gas present over the entire angular extent of SgrA East and also beyond. The 90 cm data shows zero-velocity lower-density ionized gas present along the line of sight to the Galactic center.

2. Observations of Recombination lines near 1374 and 332 MHz

Recombination lines (RL) at lower frequencies (e.g. $\nu \leq 1.4$ GHz) are sensitive to lower density extended ionized gas due to enhanced stimulated emission in such gas at higher quantum levels (Shaver 1975, Pedlar et al 1978, Anantharamaiah 1985). On the other hand, at higher frequencies ($\nu \geq 5$ GHz), it is easier to observe higher density, compact ionized regions. High resolution recombination line observations of the Galactic center region has so far been made only at frequencies above 5 GHz. (Van Gorkom et al 1985, Roberts and Goss 1993, Yusef-Zadeh et al 1995) and they have been useful in studying relatively high density ($n_e > 10^3 \text{ cm}^{-3}$) ionized gas in SgrA West, in the Arched filaments and in other compact HII regions in that area. However, the extended lower density ionized gas in the SgrA complex, for which evidence was presented in the previous section, has not been detected in high frequency recombination lines. We therefore undertook observations of the H168 α line at $\nu_{rest} = 1374.6$ MHz and the H270 α line at $\nu_{rest} = 332.25$ MHz using the VLA.

Observations at 1374 MHz were made in 1996 in both C and D configurations of the VLA using a bandwidth of 6.25 MHz and 64 channels. The velocity resolution was 21.3 km s^{-1} and the velocity coverage was $\pm 650 \text{ km s}^{-1}$. The data were edited, calibrated and imaged using standard procedures in AIPS software. The angular resolution of the final line and continuum images is $56.7'' \times 24.6''$ and PA = 35° . For the H270 α line at 332 MHz, we used the data obtained in the D configuration of the VLA in 1987 as a part of the continuum study published by Pedlar et al (1989). The velocity resolution of the data is 11.0 km s^{-1} and covers a range of $\pm 300 \text{ km s}^{-1}$. The angular resolution is $8.2' \times 3.7'$ with PA = 10° .

Fig 3 shows the spatially integrated profiles of the H168 α and the H270 α lines. The two line profiles are different which illustrate that recombination lines at different frequencies are sensitivity to different components of ionized gas. The higher frequency line (i.e. H168 α) extends over a large velocity range ($\sim 200 \text{ km s}^{-1}$) and arises in relatively higher density gas ($n_e > 100 \text{ cm}^{-3}$) close to the galactic center whereas the lower frequency line (i.e. H270 α) is narrow ($\sim 30 \text{ km s}^{-1}$) and arises in a lower density gas ($n_e < 10 \text{ cm}^{-3}$) which may be anywhere along the line of sight (Anantharamaiah and Bhattacharya 1985). Note that the expected radial velocity for the line-of-sight gas towards the Galactic Center is 0 km s^{-1} . The narrow feature near -150 km s^{-1} in the 90 cm profile is the C270 α line. The H270 α and the C270 α lines are dominated by stimulated emission (Pedlar et al 1978, Anish Roshni and Anantharamaiah 1997) and thus their spatial distribution follows that of the continuum. With the sensitivity of the present observations, the lines are clearly detected only near the continuum peak. The lower frequency line is not discussed further here since it does not arise close to the Galactic center.

The H168 α line profile in Fig 3 is consistent with single-dish measurements at this position by Kesteven and Pedlar (1977). A slight uncertainty in the baseline (i.e. the zero-level) is still visible in the spectrum which is due to the residual 3-MHz ripple in the VLA waveguide system. A significant narrow feature at a velocity of 470 km s^{-1} is present in the H168 α spectrum which needs to be confirmed by further observations.

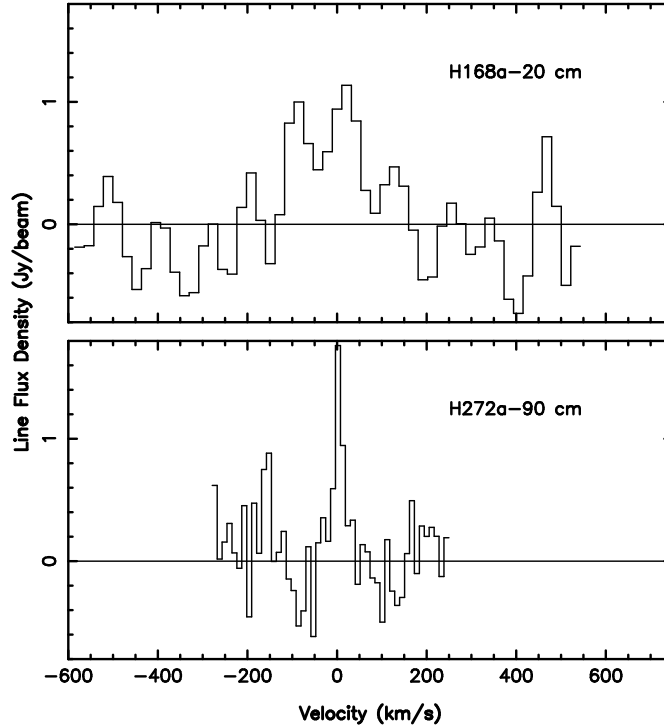


Figure 3. $\text{H168}\alpha$ (*top*) and $\text{H270}\alpha$ (*bottom*) recombination line profiles integrated over the SgrA complex. The narrow feature near -150 km s^{-1} in the lower profile is the $\text{C272}\alpha$ line.

Fig 4 shows the continuum image of the SgrA complex at 20 cm (1374 MHz) in contours with $\text{H168}\alpha$ line emission integrated over the velocity range -200 km s^{-1} to $+42 \text{ km s}^{-1}$ (moment 0) superposed in grey scale. The angular resolution is $56.7'' \times 24.6''$ with $\text{PA} = 35^\circ$. The continuum image shows the three main components of the SgrA complex: the triangular shaped outer halo which is about $10'$ in size, the shell-like structure of SgrA East and the bright central region, SgrA West. At this angular resolution, SgrA* is not separated from SgrA West. The integrated line emission in grey scale shows that the $\text{H168}\alpha$ line emission extends over the whole of SgrA East. There can be little doubt that this extended emission arises in ionized gas associated with the galactic center since the velocities are non-zero and the velocity extent of this gas is much larger than that of the line-of-sight gas detected in the $\text{H270}\alpha$ line. The detection of an extended region of $\text{H168}\alpha$ line emission is consistent with the conclusions of Pedlar et al (1989) who attributed the turnover in the spectrum of SgrA East to free-free absorption by thermal gas. There is also some weak $\text{H168}\alpha$ line emission to the north of SgrA East where the base of the arched filaments meet the SgrA halo at $(l, b) = (0, 0)$.

The velocities and spatial distribution of the $\text{H168}\alpha$ emission can be seen in the channel maps shown in Fig 5. The $\text{H168}\alpha$ emission can be identified in Fig 5 in three distinct velocity ranges. Taking into account the channel width of 21.3 km s^{-1} , these three velocity ranges are (1) $+50$ to -10 km s^{-1} , (2) -75

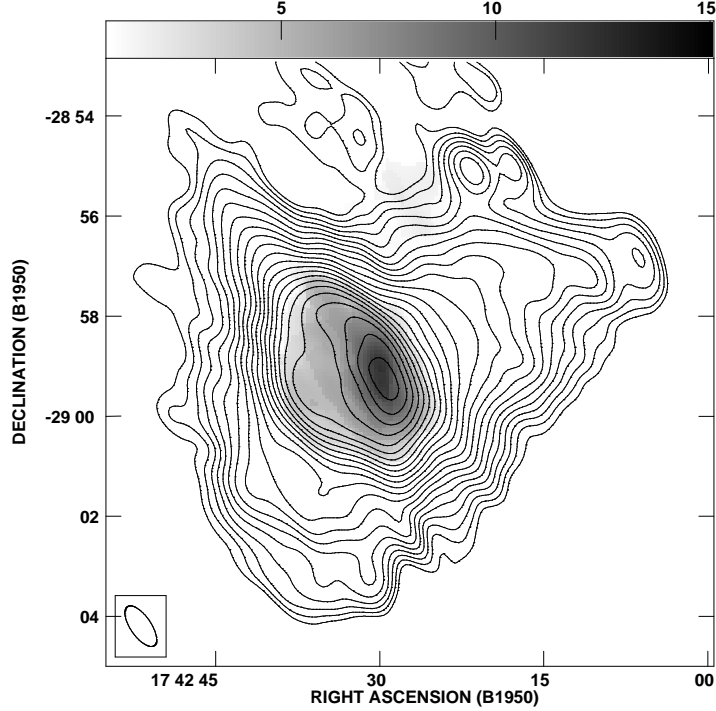


Figure 4. Continuum image of SgrA complex at 1.37 GHz in contours with H168 α line emission integrated over the range +50 to -200 km s $^{-1}$ in grey scale. The first contour level is 0.3 mJy/beam and the subsequent ones are successively higher by a factor of 1.2. The grey scale range is 1 to 15 Jy/beam km s $^{-1}$. The beam is 56.7'' \times 24.6'' and PA = 35 $^{\circ}$.

to -115 km s $^{-1}$ and (3) -180 to -200 km s $^{-1}$. In addition to these emissions, a narrow high velocity feature with $V_{lsr} = 470$ km s $^{-1}$ was detected in the spectrum shown in Fig 3. The channel image at $V_{lsr} = 470$ km s $^{-1}$ is shown in Fig 6 in contours superposed over the continuum image in grey scale. If this line emission is confirmed by further observations, then it represents in-falling ionized gas at a high velocity and extended over a few parsecs.

In the velocity ranges +50 to -10 km s $^{-1}$ and -75 to -115 km s $^{-1}$, the line emission is spread over the entire extent of SgrA East with the peak of emission in front of SgrA West. Comparing the observed velocities of the H168 α line at the position of SgrA West with the velocities observed at higher frequencies by Roberts and Goss (1993) and Yusef-Zadeh et al (1995), it appears that the H168 α line emission does not arise in the ionized gas that is directly associated with SgrA West. The ionized gas detected in the H168 α line is clearly extended and possibly lies in front of both SgrA East and West sources. The similarity of the spatial structure of line emission (which is from thermal gas) and that of SgrA East (which is a non-thermal source) strongly suggests that the H168 α line is dominated by stimulated emission. It is therefore possible that the line

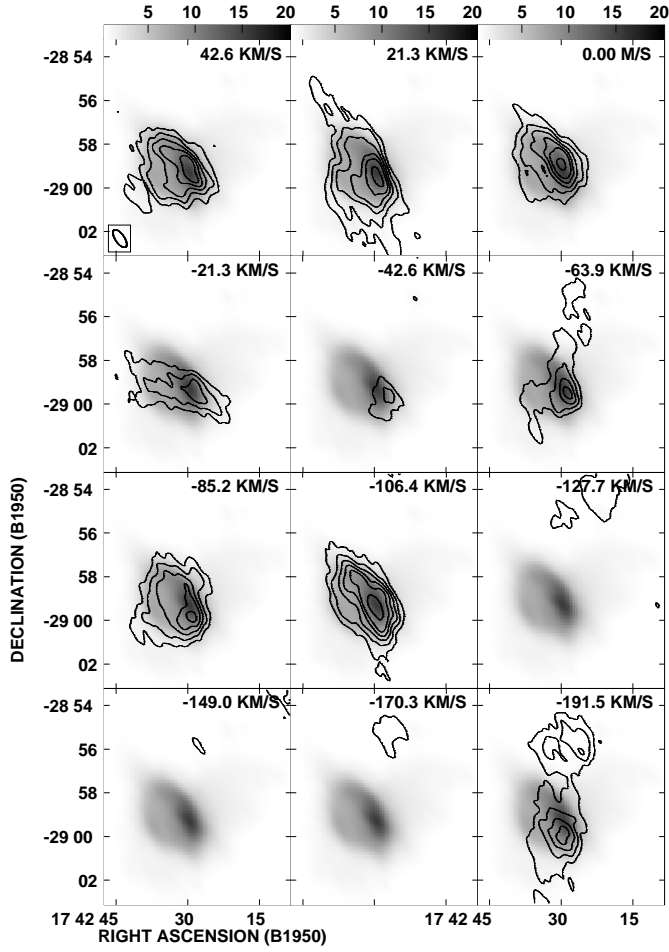


Figure 5. Channel maps of H168 α emission in contours superposed over a grey scale continuum image at 20 cm. The LSR velocities are indicated in each frame. Contour levels are 20,30,40,50,60,80 mJy/beam. The beam size is as in Fig 3.

emission extends even beyond SgrA East which may not be detected here due to lack of sensitivity and diminished background continuum. Due to limited angular and velocity resolution of these observations, no systematic motion of this gas can be discerned. Since there are three distinct velocity ranges where line emission occurs, the three regions are likely to be separated along the line of sight. Some of this ionized gas may be associated with the halo and mixed with the non-thermal gas as suggested by Pedlar et al (1989).

The peak of emission near -190 km s^{-1} occurs south of the continuum peak. Some weak emission at this velocity also occurs slightly north of SgrA East. Although negative velocities are observed in the higher frequency H92 α lines (Roberts and Goss 1993) in the southern arm of SgrA West, the H168 α line emission at this velocity is more extended than the southern arm and thus may represent a distinct component.

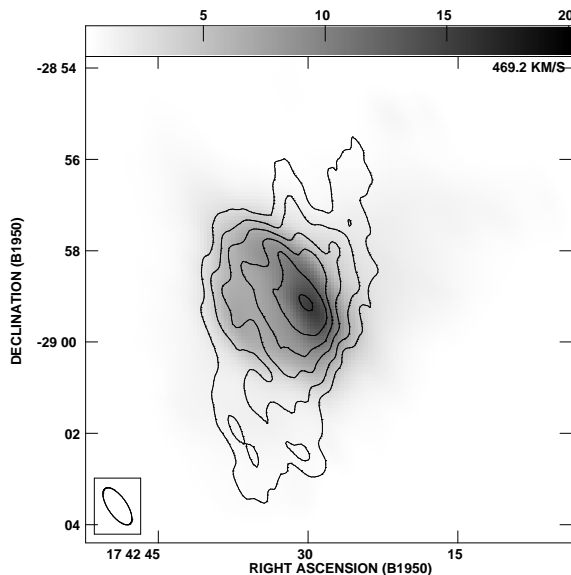


Figure 6. Channel image of the H168 α emission at $V = 470 \text{ km s}^{-1}$ (in contours) superposed over the continuum image at 20 cm. The contour levels are 20, 30, 40, 50, 60, 80 mJy/beam. The beam size is as in Fig 4.

3. Constraints on the Density and Mass of Ionized gas

The extended ionized gas observed here in the H168 α line is not observed in the lower frequency H270 α line nor in the higher frequency H110 α and H92 α lines. High resolution H110 α and H92 α VLA observations may also have missed detecting extended gas due to lack of sensitivity to such structures. As explained in Section 1, lower frequency continuum observations indicate the gas has a free-free optical depth $\tau_{ff} \sim 1$ at $\lambda = 90 \text{ cm}$. These facts allow us to place some constraints on the density and emission measure of the ionized gas.

Fig 7a shows a H168 α line profile spatially integrated over a $54'' \times 135''$ region of SgrA East centered at RA = $17^h 42^m 35.2^s$ and DEC = $-28^\circ 59' 18.0''$. This region is to the east of SgrA West and thus the line profile has no contribution from the latter. As discussed in Section 1, this region shows a turnover in the spectrum of SgrA East which is attributed to free-free absorption by thermal gas. It is reasonable to suppose that the H168 α line in Fig 7a arises in this gas. Although the line profile in Fig 7a is complex consisting of at least 3 components, for the purpose of illustration of the model, we approximate it by a Gaussian with a peak of 130 mJy/beam, FWHM = 220 km s^{-1} and a centroid near 0 km s^{-1} . The integrated line flux is $1.3 \times 10^{-21} \text{ W m}^{-2}$. The continuum flux density of SgrA East over this region is $\sim 36 \text{ Jy/beam}$ at 1.37 GHz. We assume an intrinsic spectral index of -0.9 based on higher frequency measurements (Ekers et al 1983).

To illustrate possible models which can account for the observed line emission, we assume a homogeneous slab of ionized gas at a temperature of 10^4 K to be in front of SgrA East. Fig 7b shows four models with different densities. The densities are 10 cm^{-3} for the dash-dot-dash line, 100 cm^{-3} for the solid line, 500

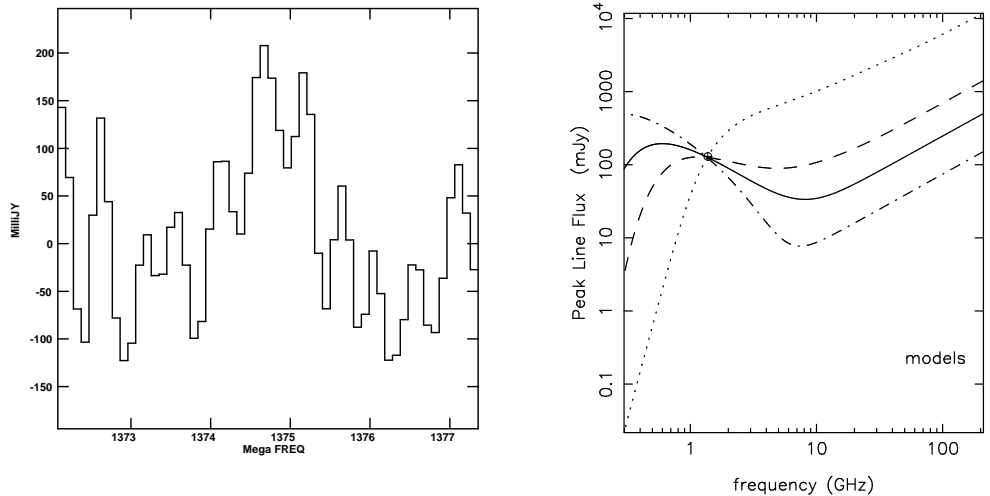


Figure 7. (a) H168 α line profile integrated over a $54'' \times 135''$ region on SgrA East at the position RA = $17^h 42^m 35.2^s$ and DEC = $-28^\circ 59' 18.0''$. At this position there is no contribution to the line from SgrA West. (b) Possible models to account for the line emission. See text for parameters of the models

cm^{-3} for the dashed line and 5000cm^{-3} for the dotted line. The emission measure in each model is adjusted to fit the observed H168 α line. It is clear from Fig 7b that the models with the highest (5000 cm^{-3}) and lowest (10cm^{-3}) densities do not produce the observed behavior. The high density model predicts a sharp increase in line strength towards higher frequencies, whereas the lower density model predicts an increase towards lower frequencies. Only the intermediate density models predict lower line strengths at both higher and lower frequencies as observed. We favor the model represented by the solid line which has $n_e = 100\text{ cm}^{-3}$, $\text{EM} = 3.3 \times 10^5\text{ pc cm}^{-6}$. This model predicts a free-free optical depth of ~ 1.1 at 90 cm consistent with the observed turnover in the spectrum of SgrA East (Pedlar et al 1989). Stimulated emission accounts for 90% of the line strength. The predicted line strengths in Fig 1 (solid line) are consistent with non-detection at 330 MHz and between 5 GHz and 10 GHz. The model also predicts that recombination lines at higher frequencies ($\nu > 10\text{ GHz}$) may be detectable. It is possible that some of the H66 α line emission near 22 GHz observed by Mezger and Wink (1986) from an 'extended' component is from this gas. In the model represented by the solid line in Fig 1b, the total mass of the ionized gas is about 10^3 M_\odot . Ionization of this gas can be maintained by a single O5 star. Note that this model, which is for illustration, is only for the ionized gas which is in front of a part of SgrA East and which is responsible for the line emission shown in Fig 7a. To account for the total line emission shown in Figs 3 and 5, it is necessary to separate the possible contribution from SgrA West.

This separation is not attempted here. If we assume that ionized gas with the same properties extends over whole of SgrA East (i.e. about 4 arminutes), then the total ionized mass is $\sim 8 \times 10^4 M_{\odot}$.

The National Radio Astronomy Observatory is a facility of the National Science Foundation operated under cooperative agreement by Associated Universities, Inc.

References

- Anantharamaiah, K.R. 1985, J. Ap. Astr., 6, 203
 Anantharamaiah, K.R. & Bhattacharya, D. 1986, J. Ap. Astr. 7, 141
 Anish Rosh, D., & Anantharamaiah, K.R. 1997, MNRAS, 292,63
 Anantharamaiah, K.R., Pedlar, A., Ekers, R.D., & Goss, W.M. 1991, MNRAS, 249, 262
 Ekers, R.D., van Gorkom, J.H., Schwartz, U.J. & Goss, W.M. 1983, A&A, 122, 143
 Kestevan, M.J. & Pedlar, A. 1977, MNRAS, 180, 731
 Lo, K.Y., Shen, Z.Q., Zhao, J.H. & Ho, P.T.P 1998 ApJ, 508, L61
 Mahadevan, R., 1998, Nature, 394, 651
 Mezger, P.G. & Wink, J.E. 1986, A&A, 157, 252
 Pedlar, A., Davis, R.D., Hart, L. & Shaver, P.A. 1978, MNRAS182, 473
 Pedlar, A., Anantharamaiah, K.R., Ekers, R.D., Goss, W.M., Van Gorkom, J.H., Schawrtz, U.J., & Zhao, J.H. 1989, ApJ, 342, 769
 Roberts, D. & Goss, W.M. 1993, ApJS, 86, 133
 Shaver, P.A. 1975, Pramana, 5, 1
 van Gorkom, J.H., Schwartz, U.J. & Bregman, J.D. 1985, IAU symp 106, The Milky Way Galaxy, ed. H. von Woerden, R.J. Allen & W.B. Burton (Dordrect:Kluwer), 443
 Yusef-Zadeh, F. & Morris, M. 1987, ApJ, 322, 721
 Yusef-Zadeh, F., Zhao, J.H & Goss, W.M. 1995, ApJ, 442, 646